

## Final Report

Grant Award Numbers: G15AP00043 and G15AP00044

Title: Probing dynamic interactions between the Haida Gwaii and Craig earthquakes and implications for Southeast Alaska faults: Collaborative Research with the University of Texas at Austin and Georgia Institute of Technology

Investigators: Jacob Walter  
University of Texas Institute for Geophysics  
10100 Burnet Road (R2200)  
Austin, TX 78758-444  
Phone: 512-232-4116  
jwalter@ig.utexas.edu

Zhigang Peng  
Georgia Institute of Technology  
311 Ferst Drive  
Atlanta, GA, 30332-0340  
Phone: (404) 894-0231, Fax: (404) 894-5638  
zpeng@gatech.edu

Term Covered by the Report: March 2015 - February 2016

Funding expended \$49,996 (UT, G15AP00044), \$45,000 (GT, G15AP00043)

## **Subtitle: Absence of and presence of static triggering of seismic activity along the Queen Charlotte-Transition Fault Zone and insights from aftershocks along the Queen Charlotte Fault near the 2013 Craig earthquake rupture**

### **1. Introduction**

The  $M_w$  7.8 (28 October 2012) Haida Gwaii earthquake and the  $M_w$  7.5 (5 January 2013) Craig, Alaska earthquake occurred just 400 km and 68 days apart from each other. The short duration and distance between the events posed the logical question of whether these two events are related. We closely studied these two events using the seismic activity prior to and following each event as a proxy to determine whether static and/or dynamic triggering of earthquakes or tremor occurs in the nucleation zone of the latter, Craig earthquake, and also regionally throughout other parts of Alaska. If seismicity is a proxy for fault movement or deformation, then we find no detectable fault deformation between the events when not previously present and when clustered, may indicate increased seismic hazard due to these large earthquakes.

In this NEHRP grant, we performed two separate network waveform cross-correlations on two separate catalogs; these were done on events originally detected separately by the Alaska Earthquake Center (AEC) and Canadian National Seismic Network (CNSN). Before the cross-correlation, we revised many phase picks and identified many new events that were originally missed. We found an increase in the seismicity rate on the Transition Fault, to the north of the Craig earthquake rupture, after the Craig mainshock. We did not detect any significant precursory seismicity that could have been triggered by the Haida Gwaii earthquake in the Craig nucleation area, though we originally hypothesized that this might have occurred (Walter et al., in prep).

We have conducted a systematic detection of remotely triggered seismicity in Eastern Denali Fault following the two mainshocks (Aiken et al., 2015). We found both short-duration high-frequency bursts during the Rayleigh waves of these events, as well as long-duration emergent tremor-like events during the Love and Rayleigh waves. We interpreted the long-duration events as triggered tremor associated with the Eastern Denali Fault, while the short-duration events as either icequakes at nearby glaciers or shallow microseismic events. Our studies suggested that the active faults in intra-plate settings are also capable of generating triggered tremor.

In addition to examining the seismicity rates using regional seismic data from two regional networks, we also closely analyzed seismic data recorded during a 21-day ocean bottom seismometer deployment of some 8 stations that recorded 2,345 aftershocks in the nucleation region of the Craig earthquake. We utilized the OBS observations to identify aftershocks and locate them along the main offshore fault trace as well as a small splay fault to the west. Further analysis of this dataset and arrival-time tomography indicates a relatively fast upper and middle crust near the Craig earthquake rupture. This has important implications for the propagation of what was suggested to be supershear rupture (e.g. Yue et al., 2013) and further analysis of these data is the focus of a forthcoming graduate student first-authored paper (Walton et al., 2016).

## **2. Data**

### **2.1. Regional land-based seismic data**

We acquired regional earthquake catalogs from the Alaska Earthquake Center (AEC), and the Canadian National Seismic Network (CNSN). We note that while a unified ANSS catalog exists, it might not be at the appropriate completeness magnitude level for our study. This is likely a result of the location of the aftershock zone being offshore and thus having a lower detection threshold (higher magnitude of completeness) in this region. The AEC catalog records a large number of Craig aftershocks, while the CNSN catalog clearly gives a more comprehensive number of events for the Haida Gwaii earthquake, though we note some questionable gaps in the data, especially during the early aftershock period.

Given the availability of seismic data in this region, we gathered the requisite data from both sources, AEC and CNSN. Next, we briefly describe the template “matched”-filter technique, to identify earthquakes that may not be readily identified due to masking or other effects. Finally, we discuss any potential dynamic links, static or dynamic triggering, between these two sequences and further north in other areas of southeast Alaska.

### **2.2. OBS seismic data**

In addition to the catalogs from the land stations, as a separate and third catalog, we analyzed data from a “rapid-response” deployment over the Craig aftershock zone. A total of 12 OBS instruments from the University of Texas Institute for Geophysics (UTIG) instrument pool were deployed for this experiment; eight instruments were recovered and/or had usable data. The instruments are short-period OBS typically used for offshore active-source experiments and thus only ran for a limited amount of time. The sensors have a natural frequency of 4 Hz and recorded for 21 days from 28 April 2013 through 19 May 2013, ~4 months after the mainshock. The array covered the southern ~100 km of the ~150 km Craig rupture with instruments spaced ~20 km apart. For this dataset, we describe our creation of the catalog, utilizing standard STA/LTA techniques, matched-filter analysis, and a discussion of the location of the events. Further detailed analysis is contained in a forthcoming manuscript (Walton et al., 2016).

## **3. Methods**

### **3.1. Methods for regional earthquake analysis**

We acquired catalog data from AEC and CNSN and utilized their picked events as templates initially (Figure 1). Based on prior experience with regional network cross-correlation (Walter et al., 2016), we bandpass-filtered the templates between 3 and 8 Hz, cut the waveforms 1 s before and 10 s after the phase arrival (P or S), and resampled the data at a 20 Hz uniform sample rate. The matched-filter technique computes the normalized cross-correlation coefficient (coefficient between -1 and 1) at each sample point for each individual template. We shift each of the normalized cross-correlation functions for each individual component backwards relative to the traveltimes of each component and stack. Detection occurs when any point within the

stacked cross-correlation function exceeds 12 times the median absolute deviation (MAD) of the daily stack. For matched-filter detections, the new event magnitude is commonly computed relative to the magnitude of the template event using the ratio between event amplitudes and assuming a logarithmic scaling between amplitude and magnitude (e.g. Walter et al., 2016).

After the initial detection of events, we visually examined (employing two undergraduate researchers) individual traces where a possible event had a MAD of 15 or greater. Most of these events with a good network correlation were identifiable visually, though was not automatically triggered, as it lacked sufficient amplitude to trigger. After manually picking body-wave phases, we used Antelope's *dbgrassoc* module to associate the event triggers and perform an initial crude event location. The matched-filter methodology was then repeated, as described above, though new events were not manually-picked the second time

Large earthquakes cause elastic deformation of the solid enhancing or decreasing Coulomb-failure stresses on adjacent portions of the same fault, which may trigger or inhibit future seismicity in the nearby region (e.g. Stein, 1999). We used the Coulomb 3.3 software developed by Ross Stein and co-authors and USGS (<http://usgsprojects.org/coulomb/>), with finite fault solutions for both mainshocks from Lay et al. (2013). We calculated the estimated increase (or decrease) in Coulomb failure stress associated with both mainshocks (Haida Gwaii and Craig) in order to discern whether adjacent portions of the fault were pushed closer (or further from) failure, in a simple Coulomb sense.

### 3.2. Methods for OBS catalog

The OBS data was processed slightly differently than the regional catalogs, though we still used the matched-filter technique. Initially, we automatically processed the OBS dataset using a short-term average/long-term average ratio trigger. The parameters were chosen to maximize the number of detections, even if they yielded many erroneous or false earthquake detection from regional earthquakes outside the Panhandle region, larger teleseism earthquakes, or other erroneous detections. We used Antelope's *dbdetect* for the automatic trigger detector on individual vertical channels for all the available stations and then used *dbgrassoc* to associate the event triggers and perform an initial crude event location. An analyst (UT undergraduate researchers Peter Dotray and Julie Gerzina employed under this grant) reviewed each of the automatic earthquake associations and each of the phases were either adjusted based on the Antelope automatic pick or extra phases on additional stations were picked if they were not automatically detected but apparent in examining the seismograms.

Next, the network matched-filter calculation, as described previously, was performed on all the data. Possible new events with high network correlation coefficients were visually-identified and re-picked at least once and then the cross-correlation was run again.

As the OBS deployment was within a small array, we utilized relative shifts in individual phases to improve the relative locations of the newly identified events, rather than assuming they have the same spatial origin as the template event. We cross-correlated individual phases of each newly detected event relative to the master template event to obtain differential timing of arrival

phases at each component and to include phase shifts when this cross-correlation coefficient exceeds 0.4. These relative phase shifts can be used in tomoDD to obtain a relative location for the newly detected event with respect to the template event.

## **4. Results**

### **4.1. Seismicity rates from regional networks**

The matched-filter processing of the earthquakes in both regions increased the completeness of the earthquake catalog (Figure 2). Within the area where the Craig earthquake initiated, we improved the earthquake catalog by an order of magnitude ( $M_c$  of 1.3 compared with 2-2.5) by finding a total of 529 earthquakes, starting with a catalog of 29 AEC-identified earthquakes. The improvement in catalog completeness is consistent with other studies that report network waveform cross-correlation improves catalogs by an order of magnitude (Schaff and Waldhauser, 2010; Walter et al., 2015; Walter et al., 2016).

### **4.2. Lack of seismicity rate increase near Craig**

We detect no significant sustained seismicity increase in the Craig mainshock area in response to the Haida Gwaii earthquake (Figure 3). This is perhaps not surprising, given that the Coulomb stress increase was minimal along the portion of the fault that eventually ruptured during the Craig earthquake (Figure 4). There was a slight increase in earthquakes here, immediately after the Haida Gwaii event, which was possibly dynamically triggered. However, we neither observed sustained seismicity in this zone nor in the area between the Haida Gwaii and Craig earthquakes.

### **4.3. Static triggering along Transition Fault Zone**

While the Coulomb stress calculation suggests a small, but positive increase in the Coulomb stress near the eventual nucleation of the Craig event after the Haida Gwaii event, the magnitude of the stress increase is much larger for the area north of the Craig earthquake, after changes in the study region following both events. The larger magnitude Coulomb stress on the Transition Fault in this area also corresponds with a rather significant increase in seismicity rate (Figure 3). The Transition Fault is an offshore tectonic boundary that separates the Yakutat block from the Pacific plate. It is not believed to have significant relative motion (between the Pacific Plate and Yakutat block) and rarely hosts large events. Rather, the Fairweather Fault in this region accommodates much of the relative motion between North America and Pacific plates. Thus, it is rather surprising that this fault was activated by the Coulomb stress increase on the Queen Charlotte/Fairweather Fault.

### **4.4. OBS aftershock seismicity and QCF velocity structure**

For the OBS aftershocks that were recorded months after the Craig earthquake, we identified and located an initial catalog consisting of 222 events that were rigorously examined with P and S arrivals re-picked manually in Antelope, using a filter of 3-15 Hz. After running the

matched-filter analysis, we were able to detect 2,123 additional events for a total of 2,345 events (Figure 5).

In map view, most seismicity appears to align with the QCF main trace as mapped on the seafloor, with deeper seismicity slightly landward. In cross-section, aftershocks indicate a near-vertical, planar feature that is likely the QCF itself. There is a linear cluster of seismicity off of the main trace and on the Pacific Plate side of the boundary, which dips steeply away from the main QCF trace. Seismic reflection data indicate several possible strike-slip fault splay or fault strands off of the main QCF fault trace (Walton et al., 2016), a feature also noted by Holtkamp and Ruppert (2015). In depth, the 2,345 aftershocks presented in this study occur dominantly at depths from 12-24 km (Figure 5). The seismogenic depths of the aftershock activity has implications for interpreting the rupture depth of the possibly supershear rupture (Walton et al., in prep).

Phase data from event arrival times were used in tomographic inversions to infer the upper and middle crustal seismic velocities, in light of the supposed supershear rupture (Yue et al., 2013; Aderhold and Abercrombie, 2015). Those tomographic results will be included in a forthcoming graduate student publication (Walton et al., 2016). Co-PI Walter devoted project time to organize the seismic databases, train the graduate student on passive seismological techniques, and provide oversight during the analysis and interpretation of the tomographic results.

## **5. Implications for stress triggering**

### **5.1. Static triggering (or lack thereof) along the QCF**

It is well-known that earthquakes can trigger other earthquakes up to thousands of kilometers away (e.g. Hill et al., 1993). The mechanism for triggering of earthquakes can either be dynamic: due to passing surface waves, or static: displacement of faults transferring static stress laterally to adjacent regions. While there is considerable debate as to which mechanisms are more efficient at triggering other events in the near field, only the dynamic stress is relevant at teleseismic distances. The short time duration (~68 days) and close distance (~250 km) between the occurrence of the events, has led to some speculation as to whether the events are linked (Gomberg, 2013).

Large earthquakes cause elastic deformation of the solid earth when their slip surfaces fail. This deformation may cause an increase or decrease of Coulomb-failure stresses on adjacent portions of the same fault or other nearby fault surfaces (e.g. Stein, 1999). Aftershock seismicity often spatially correlates with positive coulomb stress changes (e.g. Meng et al., 2013). Aftershocks are often deficient in zones of negative Coulomb stress change or so-called “stress shadows.” Figure 5 indicates that the Coulomb shear stress perhaps increased along the Fairweather and Transition Fault, following the Craig earthquake. There was a corresponding increase in seismicity mostly along the Transition Fault, offshore. However, we did not observe any evidence of static triggering in the Craig zone from the earlier Haida Gwaii earthquake.

## 5.2. Dynamic triggering along the Eastern Denali Fault

Aiken et al. (2015) presented exhaustive evidence of dynamically triggered earthquakes and tremor along the Eastern Denali Fault in Canada and near the Canada-Alaska border. While the primary mainshocks are the Haida Gwaii and Craig events, we also examined other 17 distant earthquakes recorded by 9 broadband stations in the Canadian National Seismic Network. Clear tremor-like signals were found at the southeastern portion of the Eastern Denali Fault during surface waves of several distant mainshocks (Figure 5). The durations and waveform characteristics of the triggered signals are very similar to other recently observed triggered tremors elsewhere around the world (Peng and Gomberg, 2010; Aiken et al., 2013). Hence, we inferred that these are also deep tremor signals triggered by shear displacements along the Eastern Denali Fault. In comparison, we also identified many short-duration bursts mostly occurred during the Rayleigh waves of distant mainshocks (Figure 5). They are somewhat similar to the triggered icequakes in Antarctica following the 2010 Mw8.8 Maule, Chile earthquake (Peng et al., 2014). Unfortunately, with mostly single-station recordings, we were unable to identify the source region of those high-frequency bursts.

In an earlier study, Aiken et al. (2013) also found triggered tremor along the Queen Charlotte Fault in Haida Gwaii, close to the epicenters of the 2012 Haida Gwaii mainshock. GT student Tiegan Hobbs conducted an initial visual inspection of deep tremor activity using aftershock recordings following the Haida Gwaii mainshock. Unfortunately, we were unable to distinguish between intensive aftershock signals from weak tremor-like signals (e.g., Gomberg et al., 2012). In addition, we have checked but were unable to identify any triggered tremor signals in the epicentral regions of the 2013 Craig events. Nevertheless, our studies suggested that triggered (and likely ambient) tremor likely occurred at active inland faults away from plate boundaries.

## 6. Summary

We performed a network waveform matched-filter analysis on two separate catalogs from two earthquake rupture areas. We found no evidence for static or dynamic triggering within the Craig earthquake region between the time period between the two earthquakes. We found that after the Craig earthquake, there was a significant increase in the seismicity rate that was concentrated along the Transition fault, offshore of southeast Alaska. In addition, there was evidence of dynamic triggering further north along the Denali Fault. This suggests that while it is still possible that the Craig earthquake was triggered either statically or dynamically by the Haida Gwaii earthquake, there was not substantial microseismicity associated with it. It is still plausible that some small-scale geodetic deformation occurred, though it possibly propagated aseismically. The increase in seismicity rate in other parts of Southeast Alaska after the Craig earthquake potentially increases the seismic hazard throughout a much broader area of Alaska than simply along the adjacent fault trace.

## 7. Student Support

This NEHRP grant provided partial support to GT graduate student Chastity Aiken to finish her thesis work on triggered tremor on the Eastern Denali Fault (Aiken et al., 2015). It also supported GT graduate student Tiegan Hobbs's search for ambient and triggered tremor in the aftershock zones of the 2012 Haidai Gwaii and 2013 Craig events, although we did not find any positive results that can lead to any publications.

This grant provided partial support for two undergraduate researchers, Peter Dotray and Julie Gerzina. Dotray is still currently an undergraduate at UT and Gerzina will begin a graduate student career at Princeton this fall in a Geosciences program. UT graduate student, Maureen Walton, was supported by a Fellowship and thus was not directly supported by this grant. Co-PI Walter advised Walton on the OBS dataset processing, analysis, and interpretation. This was a chapter of her PhD thesis and she is currently a Mendenhall Postdoctoral Scholar at USGS Santa Cruz supervised by Daniel Brothers.

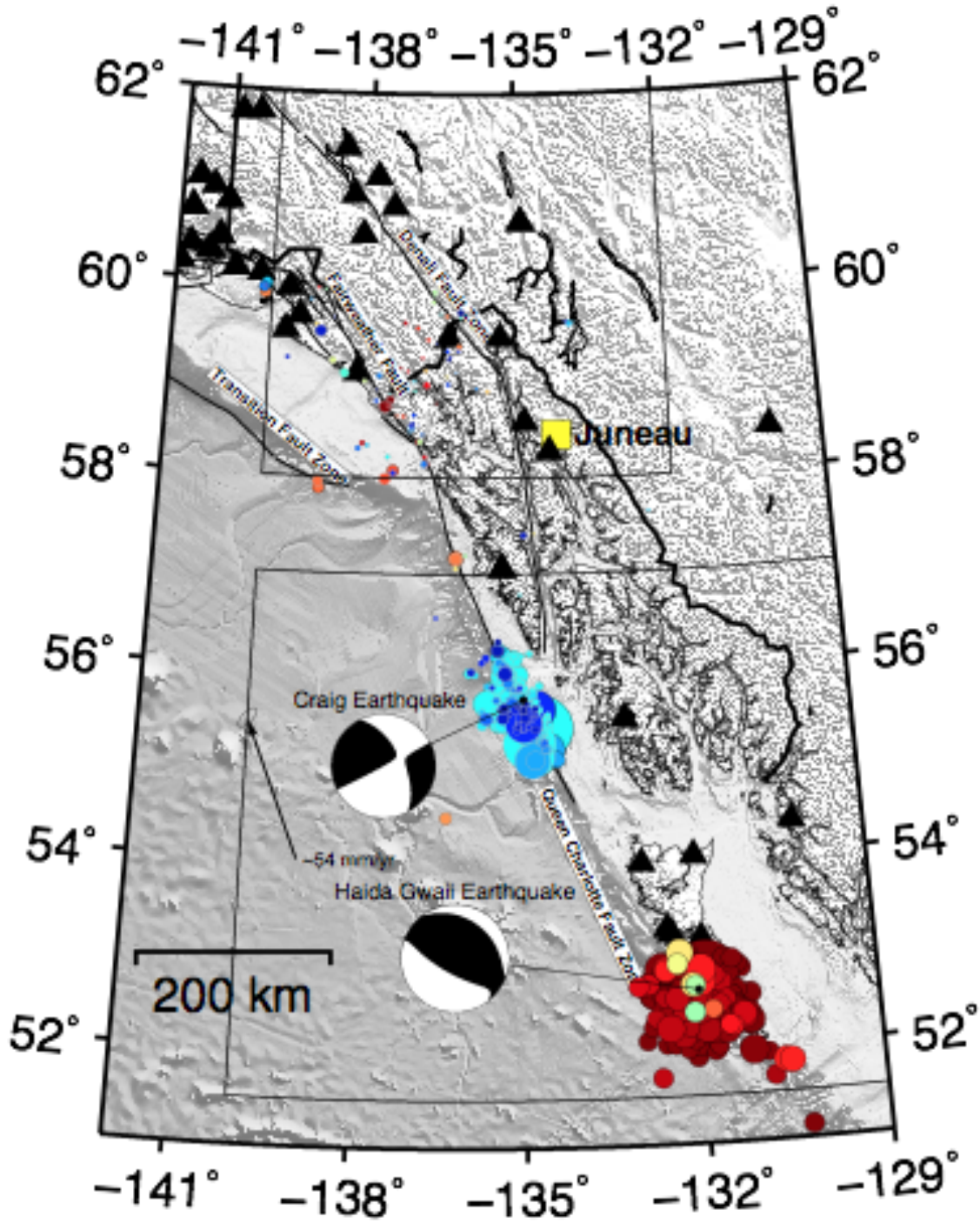


Figure 1: Southeast Alaska and Haida Gwaii Islands. Focal mechanisms of the Haida Gwaii and Craig earthquakes are provided by the Global CMT project. Color-coded aftershocks trend from hot to cold colors beginning with the Haida Gwaii earthquake timing. The approximate plate rate (~54 mm/yr) relative to a stable North America plate is shown as an arrow (DeMets et al., 2010).

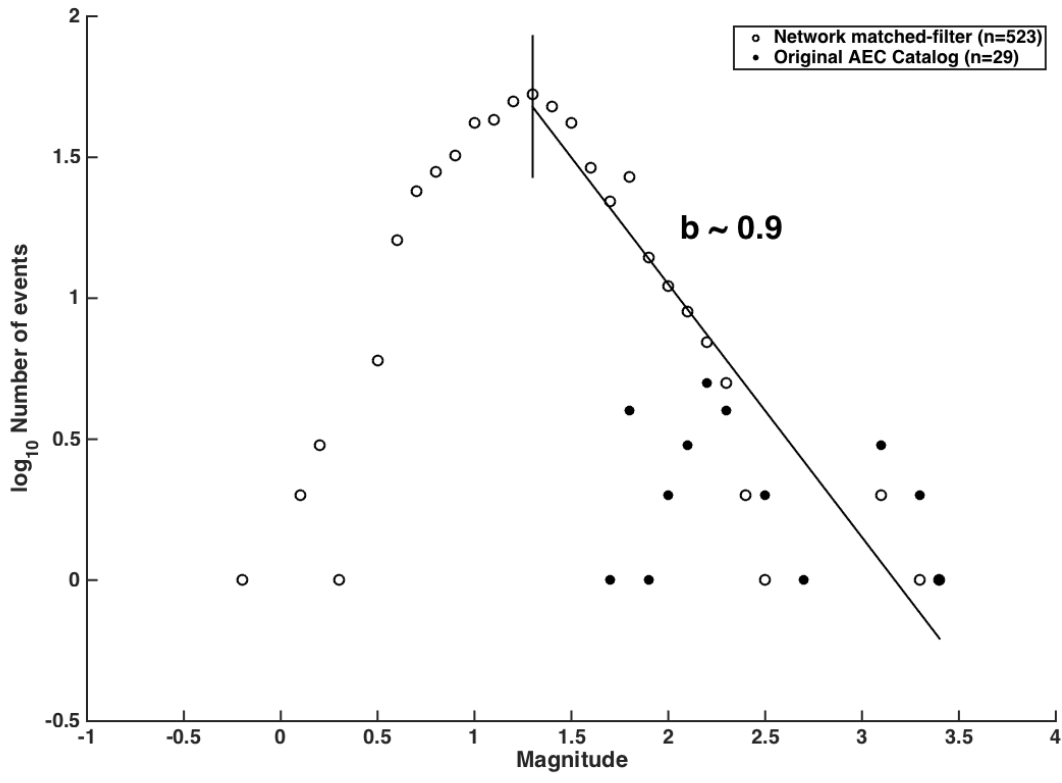


Figure 2: Matched-filter catalog improvement for zone within the Craig rupture region leading up to the Craig event. Open circles indicate catalog improvement through matched-filter detection using template earthquakes before and after the Craig earthquake. Filled circles are the AEC catalog events during the same time period. The matched-filter results suggest a completeness magnitude of 1.3, while the completeness magnitude for the AEC catalog is unclear though is likely between 2-2.5.

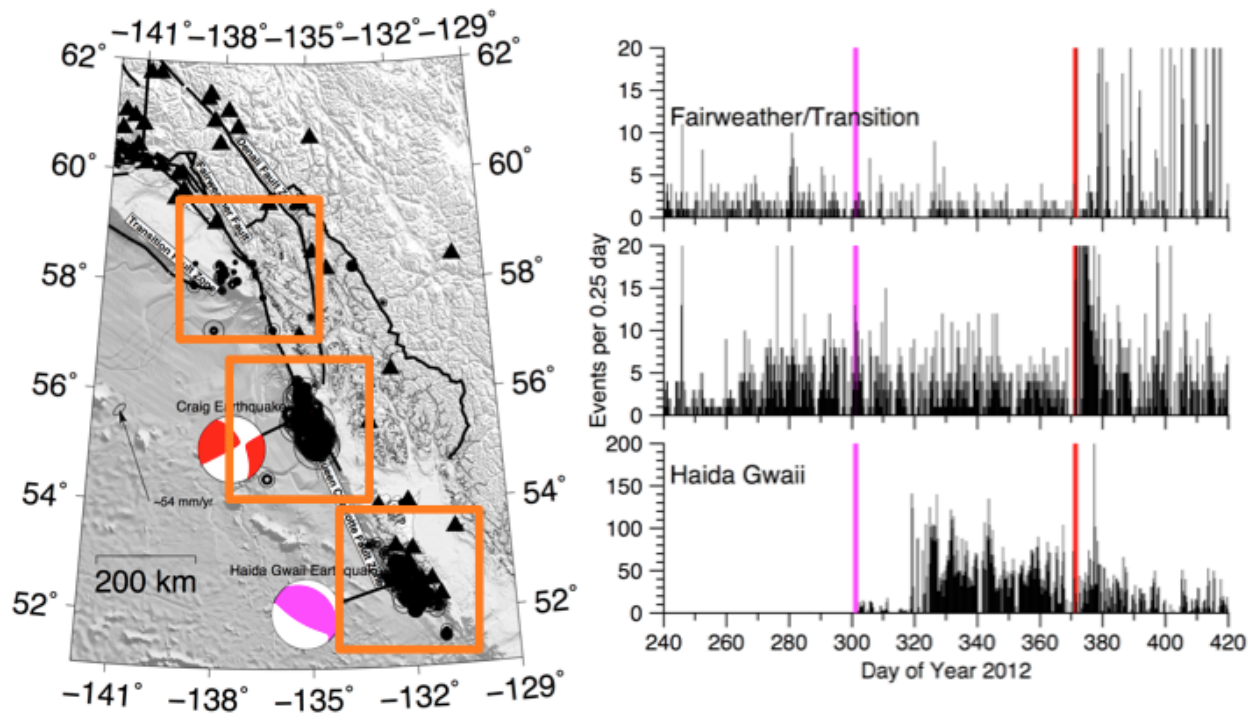


Figure 3: Seismicity in three zones along the QCF system. (Left) Map of detected seismicity along the QCF (Right top) Seismicity rate (events per 0.25 days) over time within box enclosing the Fairweather/Transition Fault. (Right middle) Seismicity rate for the Craig rupture area. (Right bottom) Seismicity rate as a function of time for the Haida Gwaii rupture area.

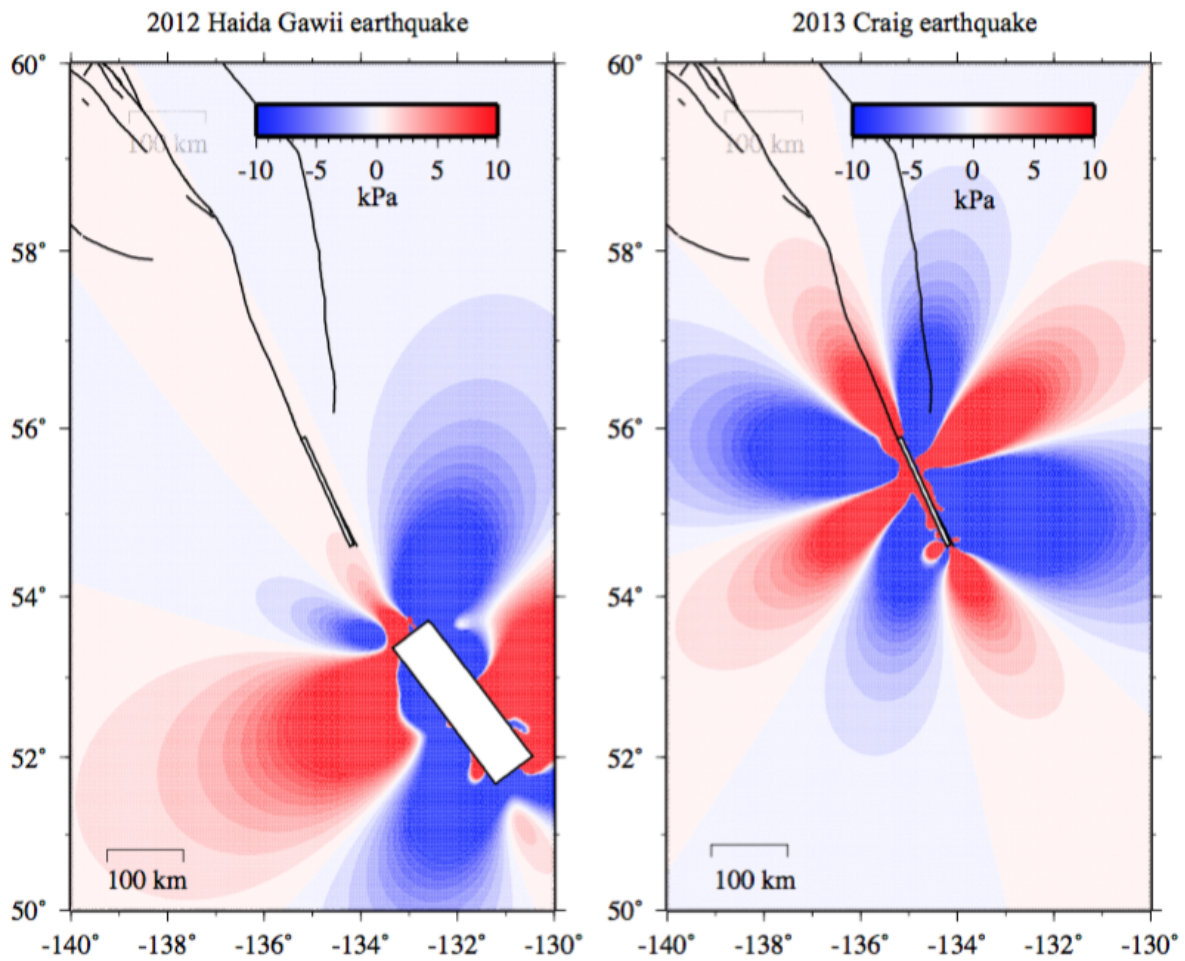


Figure 4: Coulomb stress calculated using Coulomb 3.3 software, including Global CMT fault focal mechanisms and finite fault models from Lay et al., 2013 and Yue et al., 2013 for the Haida Gwaii and Craig earthquakes, respectively.

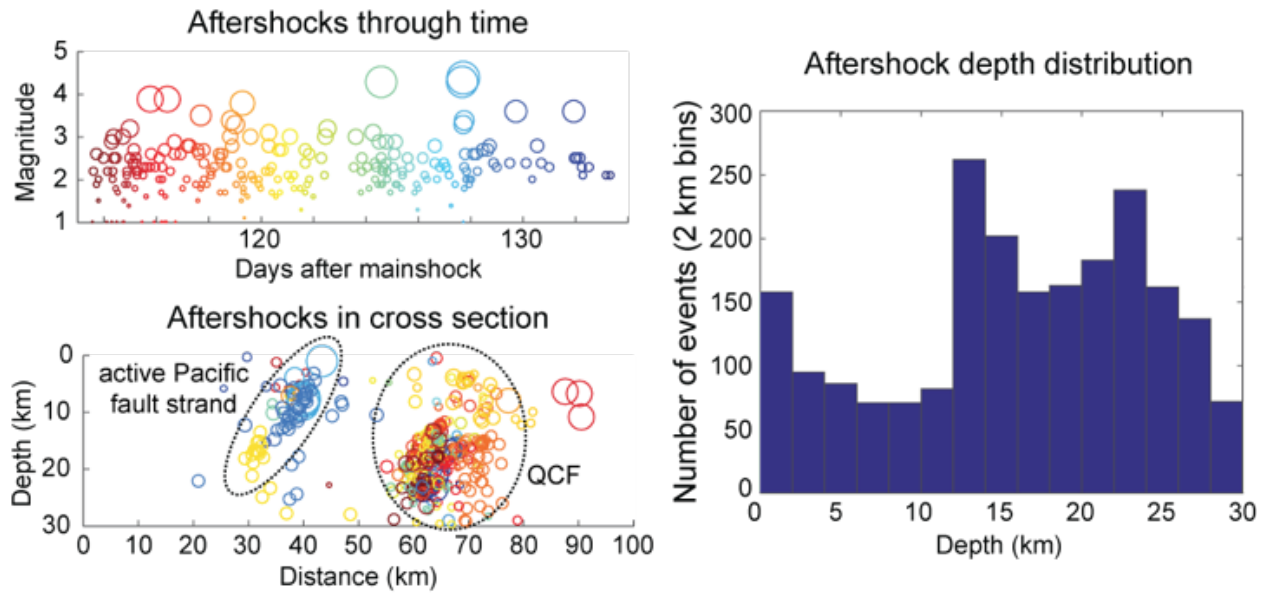


Figure 5: Aftershocks from OBS deployment, that targeted the Craig aftershock zone. (Bottom left) Cross-section perpendicular to the strike of the QCF indicates strand to the west of the main trace. (Right) Histogram of aftershock depths.

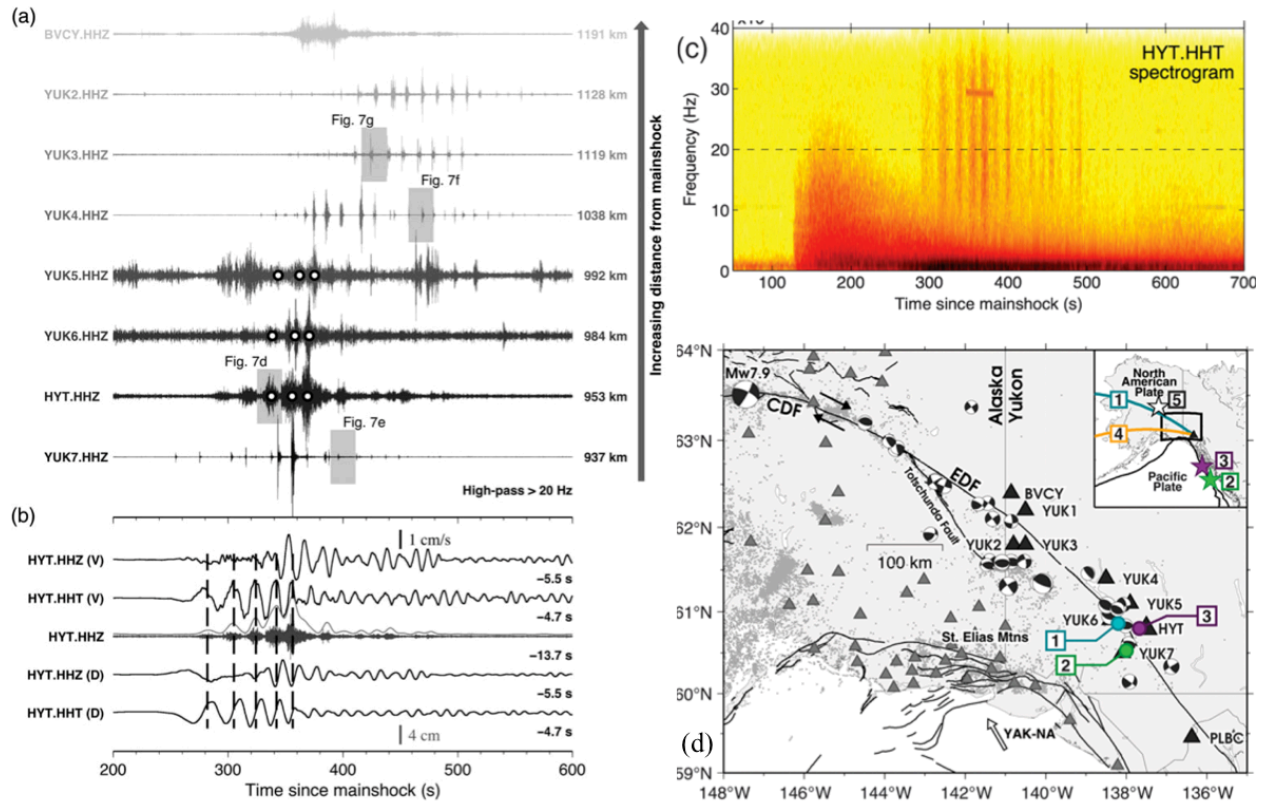


Figure 6. (a) 20-Hz high-pass-filtered seismogram showing evidence of triggered high-frequency bursts and long-duration tremor like events. (b) A comparison between triggered tremor and broadband signals. (c) A spectrogram at station HYT showing the distant mainshock signals and triggered tremor. (d) Study region in Alaska and Yukon region. After Aiken et al. (2015).

## **Bibliography supported by this grant**

### Conference Abstracts

Walter, J. I., Z. Peng, H. Kao, X. Meng, T. Hobbs, P. Dotray, T. Mulder (Oral), Dynamic interactions between the late October 2012 Haida Gwaii and early January 2013 Craig earthquakes and other faults in Southeast Alaska, AGU Fall Meeting, San Francisco, CA, December 2015.

### Manuscripts

Aiken, C., J. C. Zimmerman, J., Z. Peng, and J. Walter (2015), Triggered seismic events along the Eastern Denali Fault in northwest Canada following the 2012 Mw7.8 Haida Gwaii, 2013 Mw7.5 Craig, and two Mw>8.5 teleseismic earthquakes, *Bull. Seismol. Soc. Am.*, 105(2b), 1165-1177, doi: 10.1785/0120140156.

Walton, M. A. L., E. Roland, J. I. Walter, S. Gulick, Aftershock hypocenters and seismic tomography for the 2013 Craig, Alaska earthquake: Implications for supershear vs sub-shear rupture, *in preparation*

Walter, J. I., Z. Peng, X. Meng, et al., Static triggering of earthquakes of dormant Transition Fault offshore of southeastern Alaska, *in preparation*.

## **References**

Aderhold, K., and R. Abercrombie (2015), Seismic Rupture on an Oceanic–Continental Plate Boundary: Strike-Slip Earthquakes along the Queen Charlotte–Fairweather Fault, *Bulletin of the Seismological Society of America*, 105(2B), 1129-1142.

Aiken, C., Z. Peng and K. Chao (2013), Tectonic tremors along the Queen Charlotte Margin triggered by large teleseismic earthquakes, *Geophys. Res. Lett.*, 40, 829-834, doi: 10.1002/GRL.50020.

Aiken, C., J. P. Zimmerman, Z. Peng, and J. I. Walter (2015). Triggered seismic events along the eastern Denali fault in northwest Canada following the 2012 Mw 7.8 Haida Gwaii, 2013 Mw 7.5 Craig, and two Mw>8.5 teleseismic earthquakes, *Bull. Seismol. Soc. Am.*, 105, no. 2B, doi: 10.1785/0120140156.

Gomberg, J., S. Prejean, and N. Ruppert (2012), Afterslip, tremor and the Denali Fault earthquake, *Bull. of the Seismol. Soc. Am.*, 102, 892-899.

Gomberg, J. (2013), Permanently enhanced dynamic triggering probabilities as evidenced by two  $M \geq 7.5$  earthquakes, *Geophys. Res. Lett.*, 40, 4828–4833, doi:10.1002/grl.50933.

Hill, D. P. et al., (1993), Seismicity remotely triggered by the magnitude 7.3 Landers, California, earthquake, *Science*, 260, 1617–1623.

Holtkamp, S., and N. Ruppert (2015), A High Resolution Aftershock Catalog of the Magnitude 7.5 Craig, Alaska, Earthquake on 5 January 2013, *Bulletin of the Seismological Society of America*, 105(2B), 1143-1152.

Lay, T., L. Ye, H. Kanamori, Y. Yamazaki, K. F. Cheung, K. Kwong, and K. D. Koper (2013), The October 28, 2012 Mw 7.8 Haida Gwaii underthrusting earthquake and tsunami: Slip partitioning along the Queen Charlotte Fault transpressional plate boundary, *Earth Planet. Sci. Lett.*, 375, 57-70.

Meng, X., Z. Peng, and J. Hardebeck (2013), Seismicity around Parkfield correlates with static shear stress changes following the 2003 Mw6.5 San Simeon earthquake, *J. Geophys. Res.*, 118(7), 3576-3591, doi:10.1002/jgrb.50271.

Peng, Z. and J. Gomberg (2010), An integrative perspective of coupled seismic and aseismic slow slip phenomena, *Nature Geosci.*, 3, 599–607, doi: 10.1038/ngeo940.

Peng, Z., J. I. Walter, R. Aster, D. A. Wiens, S. Anandkrishnan, and A. Nyblade (2014), Antarctic icequakes triggered by the 2010 Maule earthquake in Chile, *Nature Geosci.*, 7, 677–681, doi:10.1038/ngeo2212.

Schaff, D.P., Waldhauser, F., 2010. One magnitude unit reduction in detection threshold by cross correlation applied to Parkfield (California) and China seismicity. *Bull. Seismol. Soc. Am.* 100 (6), 3224–3238.

Stein, R.S. (1999), The role of stress transfer in earthquake occurrence, *Nature*, 402, 605-609.

Walter, J. I., Z. Peng, X. Meng, A. V. Newman, S. Y. Schwartz, and J. Marino Protti (2015), Far-field triggering of foreshocks near the nucleation zone of the 5 September 2012 (Mw 7.6) Nicoya Peninsula, Costa Rica earthquake, *Earth and Planet. Sci. Lett.*, 431: 75-86, doi:10.1016/j.epsl.2015.09.017.

Walter, J. I., P. J. Dotray, C. Frohlich, and J. F. W. Gale (2016), Earthquakes in northwest Louisiana and the Texas-Louisiana border possibly induced by energy resource activities within the Haynesville shale play, *Seismol. Res. Lett.*, 87(2A), doi:10.1785/0220150193.

Yue, H., T. Lay, J. T. Freymueller, K. Ding, L. Rivera, N. A. Ruppert, and K. D. Koper (2013), Supershear rupture of the 5 January 2013 Craig, Alaska (Mw 7.5) earthquake, *Journal of Geophysical Research: Solid Earth*, 118(11), 5903-5919.